

# RESEARCH PAPER

## Behavior of concentrically loaded geopolymer-concrete circular columns reinforced longitudinally and transversely with GFRP bars

(Title contains 14 words)

Running headline: Behavior of concentrically loaded geopolymer-concrete circular columns reinforced longitudinally and transversely with GFRP bars (128 characters)

by

**G.B. Maranan<sup>1</sup>, A.C. Manalo<sup>1</sup>, B. Benmokrane<sup>2</sup>, W. Karunasena<sup>1</sup>, and P. Mendis<sup>3</sup>**

<sup>1</sup> Centre of Excellence in Engineered Fibre Composites (CEEFC),  
Faculty of Health, Engineering and Sciences (FoHES),  
University of Southern Queensland, Toowoomba 4350, Australia

<sup>2</sup> Department of Civil Engineering, University de Sherbrooke, Sherbrooke, Quebec,  
Canada J1K 2R1

<sup>3</sup> Department of Infrastructure Engineering, The University of Melbourne, Victoria 3010,  
Australia

Submitted to  
**Engineering Structures**

Corresponding Author:

**Allan Manalo**

Senior Lecturer in Civil Engineering (Structural)  
Centre of Excellence in Engineered Fibre Composites (CEEFC),  
Faculty of Health, Engineering and Sciences,  
University of Southern Queensland,  
Toowoomba, Queensland 4350, Australia  
Tel: +61 7 4631 2547 Fax: +61 7 4631 2110  
E-mail: [allan.manalo@usq.edu.au](mailto:allan.manalo@usq.edu.au)

**Manuscript summary:**

Total pages	33 (including 1-page cover)
Number of figures	16
Number of tables	5

# Behaviour of concentrically loaded geopolymer-concrete circular columns reinforced longitudinally and transverse with GFRP bars

G.B. Maranan<sup>1</sup>, A.C. Manalo<sup>1,\*</sup>, B. Benmokrane<sup>2</sup>, W. Karunasena<sup>1</sup>, and P. Mendis<sup>3</sup>

<sup>1</sup> Centre of Excellence in Engineered Fibre Composites (CEEFC), Faculty of Health, Engineering and Sciences (FoHES), University of Southern Queensland, Toowoomba 4350, Australia

<sup>2</sup> Department of Civil Engineering, University de Sherbrooke, Sherbrooke, Quebec, Canada J1K 2R1

<sup>3</sup> Department of Infrastructure Engineering, The University of Melbourne, Victoria 3010, Australia

Email: [ginghis.maranan@usq.edu.au](mailto:ginghis.maranan@usq.edu.au); [allan.manalo@usq.edu.au](mailto:allan.manalo@usq.edu.au); [Brahim.Benmokrane@USherbrooke.ca](mailto:Brahim.Benmokrane@USherbrooke.ca); [karu.karunasena@usq.edu.au](mailto:karu.karunasena@usq.edu.au); [pamendis@unimelb.edu.au](mailto:pamendis@unimelb.edu.au)

## Abstract

The behavior of concentrically loaded geopolymer-concrete circular columns reinforced longitudinally and transversely with glass-fiber-reinforced-polymer (GFRP) bars was investigated. Six full-scale short columns ( $L/r = 8$ ) were cast: one column without transverse reinforcement; three columns with circular hoops spaced at 50 mm, 100 mm, and 200 mm on centers; and two columns with spirals spaced at 50 mm and 100 mm on centers. In addition, two slender columns ( $L/r = 16$ ) transversely reinforced with hoops and spirals both spaced at 100 mm on centers were fabricated. Based on the experimental results, the GFRP bars contributed an average of 7.6% to the overall capacity of the tested columns. The hoop- and spiral-confined slender columns failed at a load equal to 66% and 82%, respectively, of the strength of their counterpart short columns. Irrespective of the tie configuration, the columns with higher volumetric ratios showed better compressive behavior than those with lower volumetric ratios. The ductility and confinement efficiency of the spiral-confined columns were higher than that of their counterpart hoop-confined columns. The tested columns yielded relatively superior compression performance compared to OPC-based concrete columns reinforced with GFRP bars and ties. Further studies dealing with the behaviour and slenderness limit in GFRP-reinforced geopolymer concrete slender columns are recommended to increase its uptake in the construction industry.

**Keywords:** Geopolymer-concrete columns; glass-fiber-reinforced polymer (GFRP) bars; Short columns; Slender columns; Hoops; Spirals.

---

\*Corresponding author, tel. +61 7 4631 2547; fax. +61 7 4631 2110  
E-mail addresses: [allan.manalo@usq.edu.au](mailto:allan.manalo@usq.edu.au) (A. C. Manalo)

## 1. Introduction

Fiber-reinforced-polymer (FRP) bars and geopolymer concrete have been increasingly used in the construction industry because of their many advantageous properties. Aside from being innately corrosion resistant, FRP bars are lightweight (20% to 25% of steel's density), have superior tensile strength (two to three times that of steel's yield strength), have high fatigue endurance, and are electromagnetically neutral [1-3], making them suitable as internal reinforcement for concrete structures. Geopolymer concrete, on the other hand, is a "green" material because it utilizes a geopolymer binder, rather than cement binder, that can be manufactured by the reaction of an alkaline liquid – normally a mixture of sodium silicate and sodium hydroxide solution – with industrial waste materials that are rich in silica and alumina, like fly ash (FA) and blast-furnace slag (BFS) [4, 5]. Davidovits [6] coined the generic term "geopolymer" because the chemical reaction taking place is a geopolymerization process wherein a large amount of amorphous aluminosilicate oxides reacts with alkali polysilicates yielding a polymeric Si-O-Al bonds. Geopolymers are intrinsically fire and chemical resistant, have excellent thermal stability, and exhibit low shrinkage and creep, owing to their inorganic framework [7]. Furthermore, a number of studies have shown that geopolymer concrete has mechanical properties that are either comparable or superior to that of normal concrete of the same grade [8-10]. While there are significant studies on the flexural and shear behavior of FRP-reinforced concrete (FRP-RC) [11-17], steel-reinforced geopolymer-concrete (S-RGC)

[18-23] systems, and FRP-reinforced geopolymer concrete (FRP-RGC) [24, 25], relatively few studies are available that deal with the behavior of compression members comprised of these systems [26]. In fact, among the current design guidelines and codes of practice for FRP-RC systems, only the Japan Society of Civil Engineers (JSCE) has established a design procedure for FRP-RC columns [27]. The ACI 440.1R-06 [28] does not recommend the use of FRP bars in columns while the CSA S806-12 [29] ignores the compression contribution of FRP bars, owing to their low compression contribution. Moreover, design guidelines for S-RGC systems have yet to be established.

The strength and stiffness of glass-FRP (GFRP) bars in compression, based on earlier research [30-33], ranged from 30% to 70% and from 77% to 100%, respectively, of the tension values. Paramanantham [34] tested fourteen 200 x 200 x 1800 mm GFRP-reinforced beam columns and stated that the GFRP bar was stressed to up to 20% to 30% of its ultimate strength when subjected to pure compression. Based on fifteen 450 x 250 x 1200 mm columns, Alsayed et al. [35] reported that, irrespective of the tie type (steel or GFRP), replacing the longitudinal steel bars with an equal amount of GFRP bars reduced column capacity by 13%. The results of the experimental investigation conducted by De Luca et al. [27] and Tobbi et al. [36] on a number of square columns reinforced with GRFP bars and ties revealed that the longitudinal GFRP bars contributed 5% to 10% of column capacity. The series of studies conducted by Tobbi et al. [36-38] on a number of 350 x 350 mm concrete columns with GFRP bars and ties showed that (1) the GFRP bars could be used in compression members provided that there is sufficient confinement to eliminate bar buckling; (2) GFRP ties are effective in increasing the strength, toughness, and ductility of the confined concrete core; and (3) the strength-reduction factor of 0.85 and the equations used for conventional RC columns can be adopted for GFRP-RC columns with some modifications to account for the different mechanical properties of GFRP bars compared to steel bars. Pantelides et al. [26] tested two circular columns with

internal GFRP spirals and vertical reinforcement under axial compressive loading to failure. The test results indicated that these columns achieved 84% of the axial load capacity of the all-steel control column. Afifi et al. [39] and Mohamed et al. [40] investigated the axial capacity of circular columns reinforced with GFRP bars and ties. Their study indicated that concrete columns reinforced with GFRP and steel bars behaved similarly, although the axial capacities of the GFRP-RC columns were, on the average, 7.0% lower than their counterpart steel-RC columns. Moreover, the experimental findings showed that GFRP hoops and spirals enhanced the ductility and effectively confined the concrete core in the post-peak stages. In conclusion, the research work cited indicates the suitability of concrete columns longitudinally and transversely reinforced with GFRP bars.

Some researchers have investigated the applicability of geopolymer concrete for reinforced columns. Sumajouw et al. [41, 42] tested 12 slender fly-ash-based, geopolymer-concrete columns reinforced with steel bars. Their results showed that the column capacity increased when the longitudinal reinforcement and concrete compressive strength increased. Furthermore, they stated that the current design provisions for conventional concrete could be adopted for geopolymer concrete. Sarker [43] analyzed the behavior of geopolymer-concrete columns reinforced with steel bars. He recommended that the analytical method for conventional concrete columns could be used for geopolymer-concrete columns with the appropriate stress-strain relationship of geopolymer concrete. Sujatha et al. [44] tested a total of 12 slender geopolymer-concrete column specimens reinforced with M30 and M60 grade bars. The results showed that the geopolymer-concrete columns behaved similarly to OPC columns regardless of the concrete grade, with the geopolymer concrete yielding higher load and deflection capacities and more ductile behavior than OPC.

The studies cited above demonstrate that FRP bars and geopolymer concrete are suitable materials for compression members. Moreover, combining them would yield a more

durable and more sustainable structural member with adequate strength and structural integrity. As of this writing, however, there have been only two studies that dealt with the bond behaviour of FRP bars in geopolymer concrete [45, 46], two research works about the structural behaviour of FRP-RGC beams [24, 25], and none about compression members. Thus, gaining an understanding of their structural performance is very important. This study investigated the compression behavior of geopolymer-concrete columns longitudinally and transversely reinforced with GFRP bars. The parameters considered were tie configuration (hoops and spirals), tie spacing, and slenderness ratio.

## **2. Experimental Program**

### ***2.1. Materials***

#### *2.1.1. Longitudinal and transverse reinforcement*

No. 5 high-modulus (HM) GFRP bars (CSA S807-10 [47]) with a nominal diameter of 15.9 mm (Figure 1) were used to reinforce the circular column specimens in the longitudinal direction. No. 3 HM GFRP spirals and circular hoops with a nominal diameter of 9.5 mm (Figure 2) were used to reinforce the corresponding columns transversely. These two types of lateral reinforcement are most commonly adopted for circular columns, and are the only currently available types of lateral FRP reinforcement in the market. The transverse reinforcement had an inner diameter of 180 mm. The hoops had an overlap length of 80 mm. The GFRP reinforcement was manufactured by pultruding E-glass fibers impregnated with modified vinyl-ester resin and had a sand-coated surface to enhance the bond and force transfer between the bars and the geopolymer concrete. Table 1 provides the mechanical properties of the reinforcement as reported by the manufacturer. The tensile properties of the bars were determined in accordance with the B.2 test method in ACI 440.3R-12 [48]. The tensile strength

$f_{fu}$  and elastic modulus  $E_f$  were calculated using the nominal cross-sectional area  $A_b$ . Currently, there is no standard method for determining the compressive strength of FRP bars since it is complicated due to the occurrence of fiber micro-buckling. Nevertheless, this study utilized five 15.9 mm GFRP bars, with a length of 50 mm, that were cut as flat as possible and were subjected to axial loads. Based on the test, the average compressive strength of the GFRP bars was 612.5 MPa, which was 51.7% of the bars' tensile strength. This strength ratio was comparable to that proposed by Deitz et al. [31] (50%), but was higher than that stated by Kobayashi and Fujisaki [32] (30% to 40%) for GFRP bars. In addition, this study assumed that the GFRP bars' elastic modulus in compression was similar to its elastic modulus in tension and that the tension and compression behaviour of GFRP bars was linearly elastic up to failure. These assumptions were also reported by the previous researchers.

### 2.1.2. Geopolymer concrete

A commercially produced geopolymer concrete with a proprietary mixture consisting of fine and medium sands, 10 and 20 mm coarse aggregates, plasticizer, water, and a geopolymer binder resulting from the alkali activation of two industrial waste materials – class F fly ash (FA) and ground granulated blast-furnace slag (BFS) – were used to fabricate the column specimens. All the geopolymer concrete cylinders and column specimens were cured in an ambient condition. Figure 3 shows the typical stress-strain curves of the geopolymer concrete with an average 28-day compressive strength  $f'_c$  and modulus of elasticity  $E_c$  of 38 MPa and 33 GPa, respectively, as determined in accordance with ASTM C39/C39M-15a [49]. The average slump and setting time of the geopolymer concrete, following the ASTM C143/C143M-15 [50] and ASTM C807-13 [51], respectively, were 150 mm and 90 minutes, respectively. The unique feature of this geopolymer concrete is that the entire constituent materials can be mixed in a truck bowl and remain completely dormant until the activator

chemicals are added [52]. The other mechanical properties of the geopolymer concrete were reported by Maranan et al. [24] and Aldred and Day [52].

**Table 1**  
Mechanical properties of the reinforcement.

Bar	$\phi_f$ , mm	$A_b$ , mm <sup>2</sup>	$f_{fu}$ ,* MPa	$E_f$ , GPa	$\epsilon_{fs}$ , %
No. 3	9.5	71.3	1372	65.1 ± 2.5	2.11
No. 5	15.9	197.9	1184	62.6 ± 2.5	1.89

\*Guaranteed tensile strength: average value – 3x standard deviation (ACI 440.3R-12 [48])



**Fig. 1.** 15.9 mm GFRP bars.



a. Circular hoops



a. Spirals

**Fig. 2.** 9.5 mm GFRP ties.

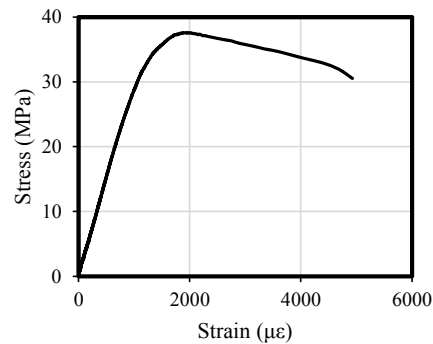


**Fig. 3.** Typical stress-strain curve of the 100 mm diameter by 200 mm high geopolymer concrete cylinder.



## 2.2. Test Specimens

Eight full-scale GFRP-RGC columns were cast and tested. One short column was fabricated without transverse reinforcement in the test region, which served as the control specimen. Three short columns reinforced with circular hoops uniformly spaced at 50, 100, and 200 mm on centers and two short columns reinforced with spirals spaced at 50 and 100 mm on centers were fabricated to investigate the influence of tie spacing and configuration. The specimen with spirals at 200 mm on centers was not considered in this study because this spacing caused the GFRP bars to buckle inward, yielding an almost hourglass-shaped reinforcement cage. In addition, two slender columns reinforced with circular hoops and spirals spaced at 100 mm on centers were produced to examine the slenderness effect. The short and slender columns had total heights ( $L$ ) of 1.0 m and 2.0 m, respectively, yielding slenderness ratios ( $L/r$ ) of 8 and 16, respectively. The  $L/r$  of 16 was practically equivalent to the slenderness limit of 17.2 suggested by Mirmiran [53], Mirmiran et al. [54], and Zadeh and Nanni [55] for GFRP-reinforced concrete columns. Figure 4 presents the specific details and configurations of the tested GFRP-RGC columns. All of the columns had a diameter of 250 mm and were reinforced with similar amounts of longitudinal reinforcement, consisting of six 15.9 mm GFRP bars, equivalent to 2.43% of the column's gross cross-sectional area ( $A_g$ ). The column height was divided into a middle test region of  $2L/3$  and two end regions of  $L/6$ . The columns' end regions were strengthened with ties spaced at 50 mm on centers to make sure that failure occurred in the test region. Figure 5 shows the actual configuration of the GFRP reinforcement cages. Figure 6, on the other hand, shows the wooden framework and the plastic-tube formwork with cast column specimens.

Table 2 depicts the column specimen identification and the test matrix. The columns were labelled as follows: GGC- $L/r$ -H(S)##. The first three letters (GGC) stand for "GFRP-reinforced geopolymer-concrete column" followed by the corresponding  $L/r$ . The next letter

represents the type of transverse reinforcement: H for circular hoops and S for spirals. The ## sign represents the hoop center-to-center spacing or the spiral pitch in millimeters. For example, the specimen identified as GGC-8-H50 is a GFRP-reinforced geopolymer-concrete column with a  $L/r$  of 8 and transversely reinforced with 9.5 mm circular GFRP hoops spaced at 50 mm on centers. The specimen labelled as GGC-8-S50, on the other hand, is a GFRP-reinforced geopolymer-concrete column with a  $L/r$  of 8 and transversely reinforced with 9.5 mm GFRP spirals with a pitch of 50 mm on centers.

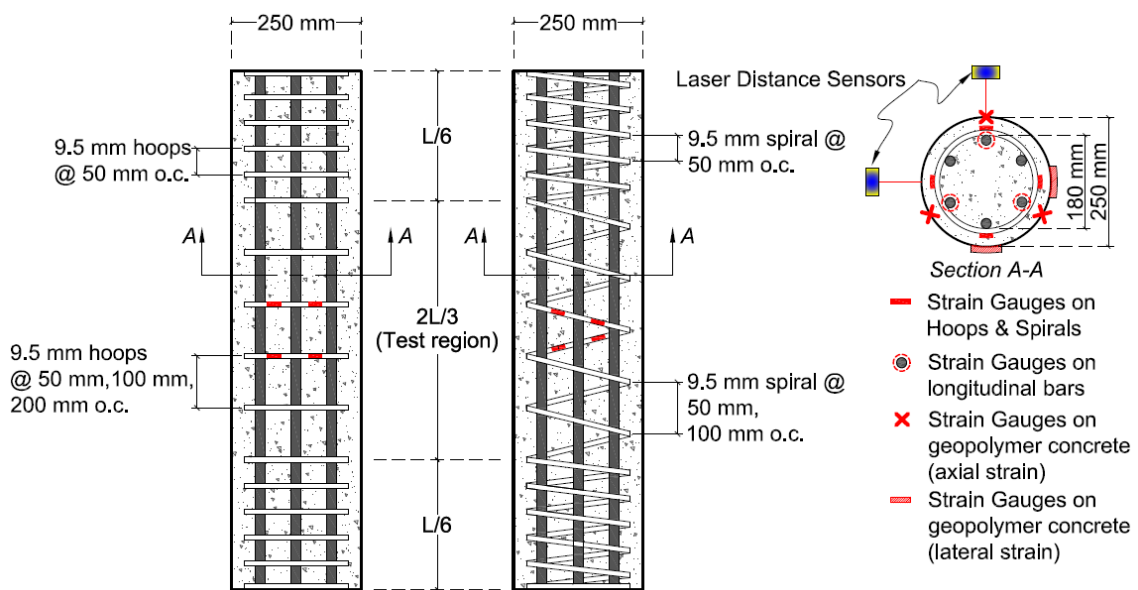


**Fig. 4.** Details and configuration of the column specimens.



a. for short columns

b. for slender columns

**Fig. 5.** Configuration of the GFRP reinforcement cages.



**Fig. 6.** Wooden framework and plastic formworks with cast column specimens.

**Table 2**

Specimen identification and test matrix.

Column	$D$ , mm	$D_c$ , mm	$\rho_f$ , %	$s$ , mm	$\rho_{fi}$ , %	$L/r$	Type
GGC-8-00	250	200	2.43	-	-	8	-
GGC-8-H50	250	200	2.43	50	3.13	8	Hoops
GGC-8-H100	250	200	2.43	100	1.57	8	Hoops
GGC-8-H200	250	200	2.43	200	0.78	8	Hoops
GGC-8-S50	250	200	2.43	50	3.13	8	Spirals
GGC-8-S100	250	200	2.43	100	1.57	8	Spirals
GGC-16-H100	250	200	2.43	100	1.57	16	Hoops
GGC-16-S100	250	200	2.43	100	1.57	16	Spirals

### **2.3. Test Program and Instrumentation**

Figure 7 shows the test setup and instrumentation employed to investigate the compression behavior of the GFRP-RGC column specimens. The columns were supported at both ends with two pairs of 10 mm thick steel collars/clamps, with an inner radius of 127 mm, to confine the top and bottom of the columns to prevent end crushing, thereby ensuring failure at the test region. Three-millimeter-thick neoprene rubber were also provided to fill the gaps between the

clamps and specimens, thereby ensuring that the end regions were properly confined. The top and bottom ends were smoothed and levelled evenly during the casting process and were provided with 3 mm thick neoprene rubber during testing to ensure uniform distribution of the applied load across the cross section. Furthermore, chicken wire was placed around the column specimens for safety purposes.

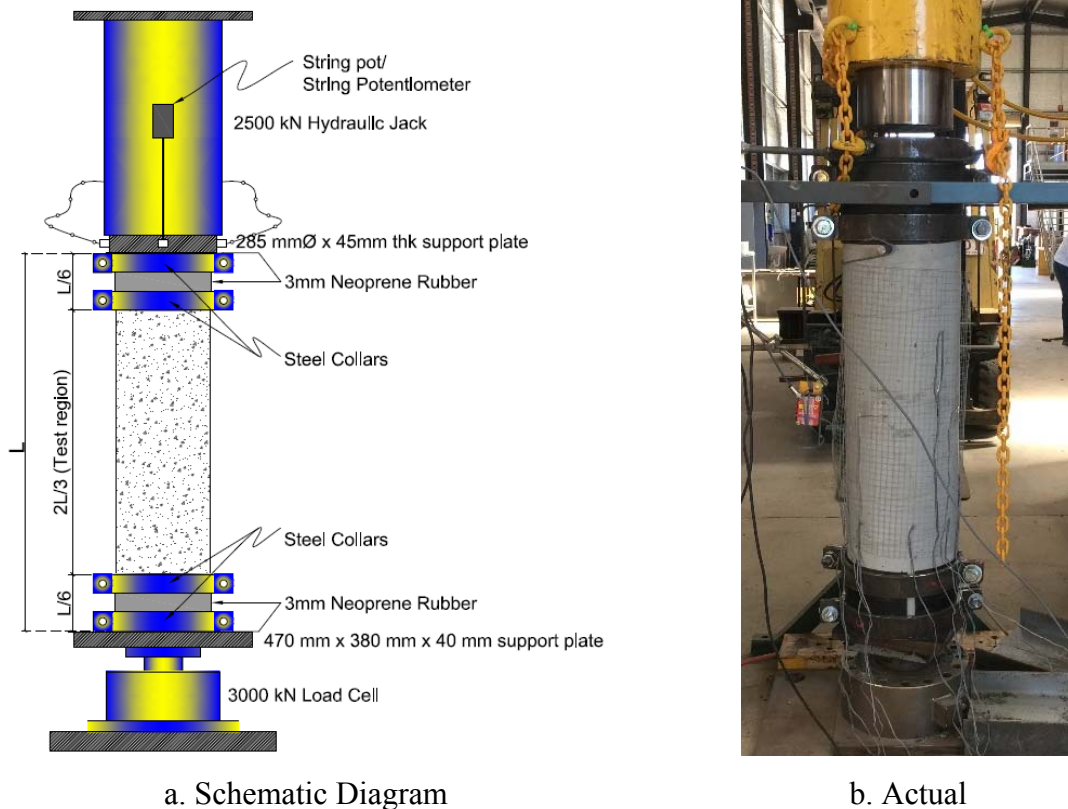


**Fig. 7.** Test Set-up.

Figure 4 provides the location of the electrical strain gauges. Three strain gauges were mounted onto three longitudinal bars to capture their compression contribution. Another three strain gauges were attached to the geopolymer concrete to measure the concrete strain; the strain gauges were positioned/aligned with the strain gauges on the bars. Four strain gauges set 90° apart were also used to capture the strains in the transverse reinforcement. All the strain gauges were positioned at mid-height of the test region. Two laser displacement sensors (LDSs) set 90° apart were used to record the columns' lateral deformations and/or lateral deflections. The columns were subjected to monotonically increasing axial concentric loads and were

loaded to failure in displacement control with a hydraulic jack to allow for the observation of both the pre- and post-peak behavior. The magnitude of the applied loads was measured with a 3000 kN capacity load cell, whereas the corresponding deformations were measured with a string pot. The strain, load, and deflection readings were recorded with a data logger attached to the machine, while the failure modes were documented with a video recorder.

### 3. Experimental Results

#### 3.1. Load–Deformation Response

Figure 8 shows the relationships between the axial load and the deformation of the tested columns. The load–deformation of the unconfined short column (GGC-8-00) consisted only of a relatively linear ascending segment, with a stiffness of 301 kN/mm, up until the peak load level, denoted as  $P_g$  in this study.  $P_g$  represents the gross capacity of the geopolymer-concrete column or the column’s capacity before concrete cover spalling. After exceeding  $P_g$ , the column failed suddenly and did not show any post-peak behavior.

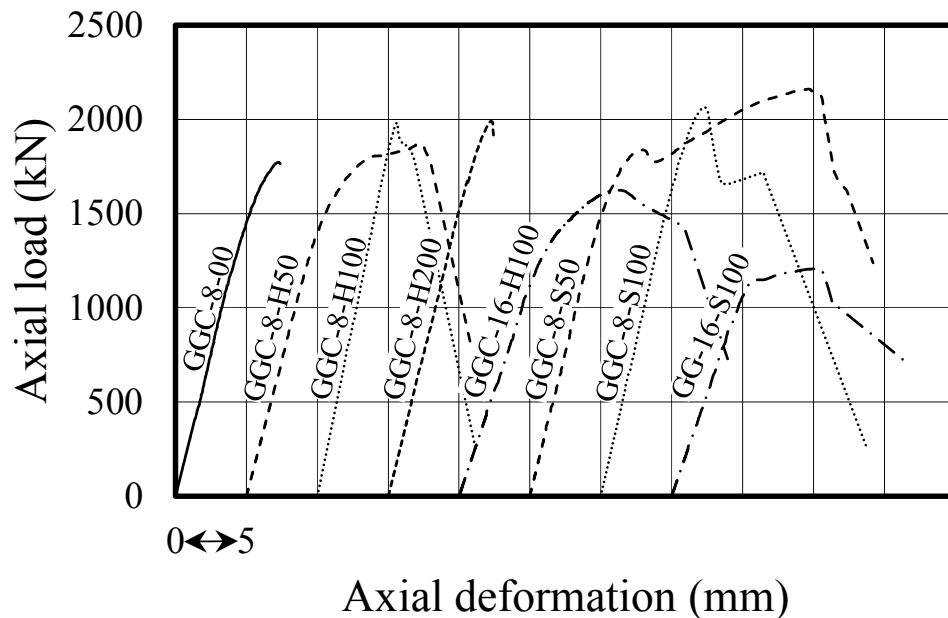


**Fig. 8.** Load-deformation response of the specimens.

The load–deformation responses of GGC-8-H50, GGC-8-H100, GGC-8-S50, and GGC-8-S100 can be divided into three phases. The first phase was comparable to that of GGC-8-00, a relatively linear load–deformation relationship with an average stiffness of 318 kN/mm. This can be expected since, at this stage, the columns’ behavior was governed predominantly by the geopolymer concrete’s compressive properties with little or no significant contribution from the GFRP ties. Furthermore, to activate the passive confinement of the GFRP ties, a higher magnitude of applied loads was needed due to the low elastic-modulus characteristics of these ties. Upon exceeding a load level approximately equivalent to GGC-8-00’s  $P_g$ , microcracks were formed causing the lateral expansion of the geopolymer concrete that subsequently yielded vertical hairline cracks on the concrete surface. At this stage, the passive confinement of the lateral reinforcement was marginally activated. A short nonlinear segment with reduced slope occurred prior to  $P_g$  owing to simultaneous crushing and cracking of the geopolymer concrete. Right after exceeding  $P_g$ , the concrete cover began to spall, producing a short descending branch that represents the second phase response of the columns. These columns, except GGC-8-H200, continued to sustain additional loads owing to the still-intact concrete core confined by lateral ties as represented by ascending or descending lines, depending on the amount of transverse reinforcement. This behavior represents the third phase response. A second peak load  $P_c$  was recorded that corresponds to the maximum load capacity of the confined geopolymer-concrete core. This load level also marks the initiation of geopolymer-concrete core crushing failure. The load-deformation response of GGC-8-H200, on the other hand, consisted only of two phases: a linear load-deformation response and a short descending branch.

GGC-16-H100 and GGC-16-S100 columns yielded similar initial linear load–deformation curves, although their initial stiffness (221 kN/mm) was lower compared to the GGC-8 columns. This is expected since the axial stiffness is inversely proportional to the height

of the column. These columns also showed more noticeable nonlinear behavior and stiffness degradation before reaching their  $P_g$  compared to their counterpart GGC-8 columns.

### **3.2. Failure Mode**

Figures 8 shows the post-failure overview of the tested columns, while Figure 10 displays the specific failure of each material. As can be expected, the specimens failed by either crushing failure or buckling failure depending upon the slenderness ratio, suggesting the effectiveness of the design and construction procedure employed in the study. Right after reaching  $P_g$ , GGC-8-00 failed suddenly through the simultaneous crushing of the geopolymer concrete and global buckling of the GFRP bars (Figure 10a). The columns failed in a brittle manner accompanied with an explosive sound. A well-formed cone on both ends (Figures 8a) characterized GGC-8-00's post-failure configuration.

The failure of GGC-8-H200 commenced with the formation of vertical hairline cracks at an applied load approximately equivalent to GGC-8-00's  $P_g$ . Since the columns had poor confinement, the longitudinal bars started to deflect laterally that contributed further to the splitting of the geopolymer-concrete cover. Upon reaching its  $P_g$ , simultaneous crushing of the geopolymer-concrete core and buckling of the longitudinal bars occurred. Concrete-cover spalling and concrete shearing outward along the inclined plane (Figure 9d) typified GGC-8-H200's failure, with relatively more intact geopolymer-concrete core compared to GGC-8-00, owing to the presence of circular ties.

GGC-8-H50 (Figure 9b), GGC-8-H100 (Figure 9c), GGC-8-S50 (Figure 9e), and GGC-8-S100 (Figure 9f), on the other hand, failed in a relatively ductile and more complex manner compared to the other columns. The failure can be described, generally, as the sequential occurrence of the following mechanism. The concentric compression load induced longitudinal strains that yielded transverse tensile strains due to Poisson's effect. At higher load levels, the

axial strains and Poisson's effect increased, thereby increasing the geopolymer concrete's lateral strain, which consequently induced the formation of vertical columnar hairline cracks on the concrete surface. These cracks progressively widened and increased in number prior to  $P_g$ , as shown in Figure 9b. More but narrower cracks were formed with increasing amounts of transverse reinforcement. After the concrete cover spalled, the geopolymer-concrete core underwent significant cracking, followed by the lateral expansion of the core, again, due to Poisson's effect. The longitudinal GFRP bars, on the other hand, started to kink and to delaminate due to the closely spaced ties preventing the bar lateral movement (Figure 10c). These events were subsequently followed by GFRP-bar rupture, geopolymer-concrete core crushing, and lap-splice joint failure of the GFRP hoops (Figure 10c) or rupture of the GFRP spirals (Figure 10d), specifically at the intersection of the longitudinal and transverse reinforcement.

GGC-16-H50 (Figure 9g) and GGC-16-S50 (Figure 9f) underwent cracking and crushing mechanisms similar to that of their counterpart short columns before reaching ultimate failure. The failure of these columns, however, was governed by column buckling and not by the crushing or shear failure of the concrete, as shown by post-failure curvature/shape of the specimens.

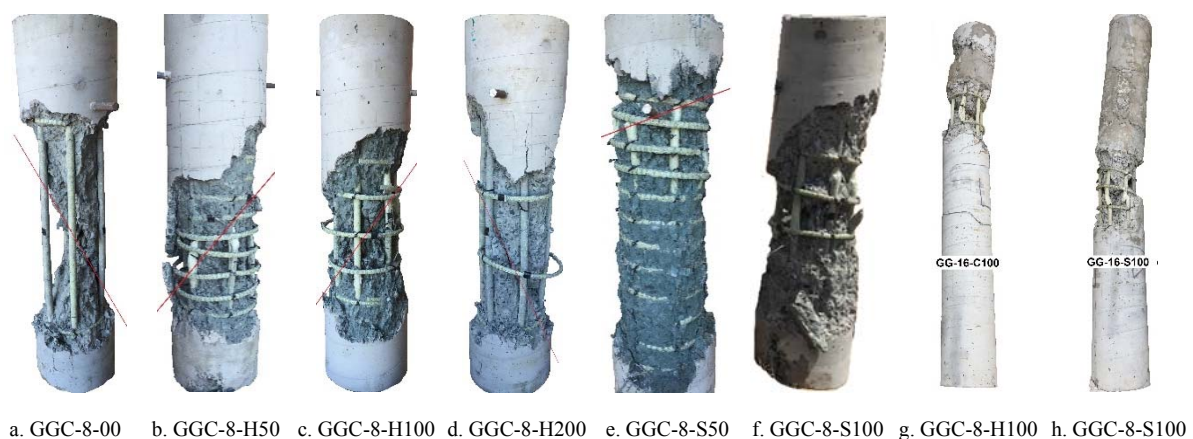


**Fig. 9.** Overview of the column specimens after failure.



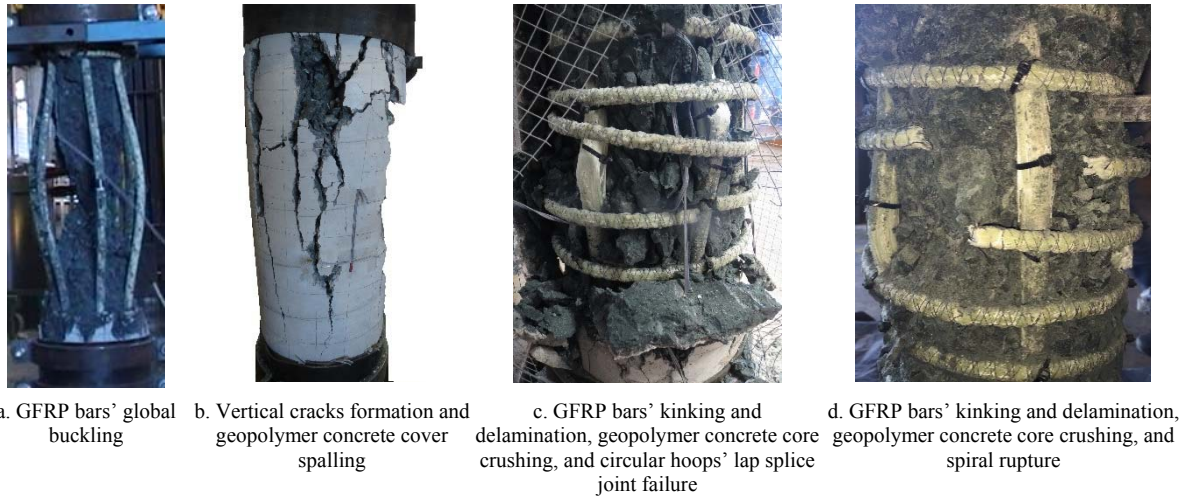


**Fig. 10.** Different failure mode configurations of the column specimens

### 3.3. *Strength and Deformation Capacity*

Table 3 summarizes the gross concrete and concrete-core load capacities ( $P_g$  and  $P_c$ , respectively) of the tested columns. The  $P_g$  of GGC-8-00 was 1772 kN. The geopolymer concrete's strength was calculated by subtracting the compression contribution of the GFRP bars from this load and then dividing the remaining load by the difference between the geopolymer concrete's gross area and total bar area ( $(P_g - P_{fg}) / (A_g - A_f)$ ). The resulting strength was equivalent to 34.42 MPa, which was approximately 90% of the average compressive strength of the standard geopolymer-concrete cylinders used in the study. Interestingly, this ratio was higher than the commonly used value of 85% for estimating the theoretical capacity of ordinary-concrete column sections, which tends to support Maranan et al.'s [24] conclusion that geopolymer concrete has better mechanical properties than ordinary portland-cement concrete of the same grade such as higher elastic modulus (leading to its better compatibility with GFRP bars compared to normal concrete), greater ultimate compressive strain (as much as  $4800 \mu\epsilon$ ), and larger tensile strength. The use of lateral ties, however, increased the  $P_g$  of GGC-8-00. GGC-8-H50, GGC-8-H100, and GGC-8-H200 yielded  $P_g$  values of 1791 kN, 1981 kN, and 1988 kN, respectively, which translated into strength increases of 1%, 12%, and 12%, respectively. Similarly, the  $P_g$  of GGC-8-S50 (1838 kN) and GGC-8-S100 (2063 kN) increased

by 4% and 16%, respectively. As mentioned earlier, this enhancement could be attributed to the activation of the lateral confining pressures of the circular hoops or spirals right after a load level approximately equivalent to GGC-8-00's  $P_g$  had been achieved. The  $P_g$  of GGC-8-H50 and GGC-8-S50 were relatively low compared to the columns with lower volumetric ratios. Given that the  $P_g$  was mainly dependent on the geopolymer concrete, this result could be due to the presence of closely spaced ties that caused discontinuity of the geopolymer concrete between the cover and core, making the column more susceptible to early concrete-cover spalling. Only GGC-8-H50, GGC-8-H100, GGC-8-S50, and GGC-8-S100, however, yielded  $P_c$  of 1872 kN, 1763 kN, 2160 kN, and 1691 kN, respectively, which were 105%, 89%, 118% and 82% of their respective  $P_g$ . As can be expected, the well-confined columns (GGC-8-H50 and GGC-8-H100) yielded  $P_c$  that were higher than their  $P_g$ . The columns with spiral reinforcement, in general, produced higher  $P_g$  and  $P_c$  compared to their counterpart circular-tie-reinforced columns. GGC-16-H100 and GGC-16-S100, on the other hand, reached  $P_g$  of 1624 kN and 1208 kN, respectively, which were just 90% and 64%, respectively, of that of GGC-8-H100 and GGC-8-S100, respectively. This result could be expected since these columns failed due to buckling, a geometric type of failure, and not by compressive or shear failure.

Table 3 summarizes the GFRP bars' compression contribution at  $P_g$  load level ( $P_{fg}$ ), which was determined by multiplying the measured average longitudinal bar strain ( $\epsilon_{fg}$ ) with the total nominal area ( $A_f$ ) and elastic modulus ( $E_f$ ) of the GFRP bars.  $P_{fg}$  represents the maximum compression contribution of the GFRP bars since the bars yielded an almost plateau behavior right after reaching this load level. The control specimen GGC-8-00 yielded the lowest  $P_{fg}$  of 123 kN, while those with lateral ties obtained  $P_{fg}$  ranging from 133 kN to 188 kN. The columns with widely spaced lateral ties (GGC-8-H100, GGC-8-H200, and GGC-8-S100) yielded an average  $P_{fg}/P_g$  of 6.9%, which was similar to GGC-8-00, whereas those with

closely spaced lateral ties (GGC-8-H50 and GGC-8-S50) produced higher  $P_{fg}/P_g$  than GGC-8-00, with an average of 9.5%. The  $P_{fg}$  of GGC-16-H100 and GGC-16-S100 were 107 kN and 143 kN, respectively, which is generally lower than their counterpart GGC-8 columns. Nevertheless, it can be generalized from these results that the longitudinal GFRP bars made a notable compression contribution and that it could be enhanced through the provision of adequate lateral confinement. This generalization contradicts De Luca et al.'s [27] findings that the compression contribution of GFRP bars was less than 5% of column capacity. Hence, they concluded that the bar contribution could be ignored when evaluating the nominal capacity of an axially loaded square RC column. This could be related to the lower longitudinal reinforcement ratio (1.0%) they used and the better mechanical properties of the GFRP bars used in this study compared to the bars they used for their research work.

Table 3 also provides the axial deformation at  $P_g$  and  $P_c$  load levels ( $\Delta_g$  and  $\Delta_c$ , respectively). Except for GGC-8-H100 (5.6 mm), all the transversely reinforced GGC-8 columns produced  $\Delta_g$  values that were higher than that of GGC-8-00 (7.2 mm). GGC-8-H100 yielded a lower axial deformation than GGC-8-00 because the former column exhibited less severe cracking, prior to reaching its peak capacity, compared to the latter column, owing to the circular hoops that restrained the expansion of concrete core and delayed the formation of cracks. The  $\Delta_g$  of the hoop-confined columns were in the following increasing order: GGC-8-H100 (5.6 mm), GGC-8-H200 (7.3 mm), and GGC-8-H50 (8.6 mm), respectively. The axial deformation of GGC-H-100 was lower than GGC-8-H200 because the former column had higher volumetric ratio, resulting to a larger volume of effectively confined geopolymer concrete; hence, the premature dilation of the core was prevented and the formation of cracks was delayed. The well confined column (GGC-8-H50), on the other hand, had denser arrangement of the steel cage that produced planes of weakness between the cover and core, and hence, this column yielded a larger axial deformation than GGC-8-H100. This was also

the reason why the axial deformation of GGC-8-S50 (8.0 mm) was greater than that of GGC-8-S100 (7.2 mm). GGC-16-H100 and GGC-16-S100, on other hand, achieved  $\Delta_g$  of 14.1 mm and 12.9 mm, respectively, which are higher than that of GGC-8-H100 and GGC-8-S100, respectively. The  $\Delta_c$  of GGC-8-H50 (12.1 mm), GGC-8-H100 (6.9 mm), GGC-8-S50 (19.7 mm), and GGC-8-S100 (11.4) were approximately 1.41, 1.23, 2.46, and 1.57 times that of their corresponding  $\Delta_g$ , respectively. Obviously, the column with higher volumetric ratio or lower tie spacing, irrespective of the tie configuration, demonstrated better deformability performance compared to those with lower volumetric ratios. Furthermore, the column with spiral reinforcement showed higher deformability compared to that with circular ties. The  $\Delta_g$  of GGC-16-H100 (11.09 mm) and GGC-16-S100 (10.39 mm) were greater than their counterpart short columns.

**Table 3**  
Peak loads and the corresponding deformations.

Column	$P_g$ , kN	$P_c$ , kN	$P_{fg}$ , kN	$\Delta_g$ , mm	$\Delta_c$ , mm
GGC-8-00	1772	-	123	7.2	-
GGC-8-H50	1791	1872	188	8.6	12.1
GGC-8-H100	1981	1763	133	5.6	6.9
GGC-8-H200	1988	-	134	7.3	-
GGC-8-S50	1838	2160	158	8.0	19.7
GGC-8-S100	2063	1717	147	7.2	11.4
GGC-16-H100	1624	-	107	11.1	-
GGC-16-S100	1208	-	102	10.4	-

### 3.4. Geopolymer Concrete and GFRP Reinforcement Strains

Figure 11 shows the relationships between the axial load and the average axial strains in the geopolymer concrete. These strains were similar for all the tested columns up until an applied load approximately equivalent to 81% of GGC-8-00's  $P_g$ . Table 4, on the other hand, shows the maximum average strains in the geopolymer concrete at the  $P_g$  load level or the average concrete strain when the cover began to spall ( $\epsilon_{cg}$ ). Right after reaching its  $P_g$ , GGC-8-00 failed suddenly at a  $\epsilon_{cg}$  of 1424  $\mu\epsilon$ . The  $\epsilon_{cg}$  of the GGC-8 columns, however, varied from 1776  $\mu\epsilon$  to

2183  $\mu\epsilon$ . These strain values were larger than GGC-8-00's  $\epsilon_{cg}$ , owing to the transverse reinforcement that prevented the premature cracking within the specimen and prevented the early buckling of the GFRP bars. Interestingly, the average  $\epsilon_{cg}$  of the tested short columns  $\epsilon_{cg-ave}$ , equivalent to 2032  $\mu\epsilon$ , was comparable to that of the normal concrete (2000  $\mu\epsilon$ ) suggested by Afifi [56] and Saatcioglu [57]. The  $\epsilon_{cg}$  of GGC-16-H100 and GGC-16-S100 were 1266  $\mu\epsilon$  and 637  $\mu\epsilon$ , respectively, which is generally lower than their counterpart short columns.

Figure 12 displays the relationships between the axial load and the axial compression strains in the longitudinal bars. As with the geopolymer concrete's strains, at the same load levels, relatively comparable strain readings were obtained from all specimens up until 81% of GGC-8-00's  $P_g$ . The figure clearly shows that the GFRP bars maintained their integrity and load resistance until after the surrounding concrete was crushed and spalled off after the peak load. Table 4 summarizes the strains in the longitudinal GFRP bars at  $P_g$  load level ( $\epsilon_{fg}$ ). The  $\epsilon_{fg}$  of GGC-8-00 was 1647  $\mu\epsilon$ , which is equivalent to 8.7% of the GFRP bars' ultimate tensile strain  $\epsilon_f$ . Generally, the GFRP ties enhanced the  $\epsilon_{fg}$  of the short columns. The  $\epsilon_{fg}$  of GGC-8-H100 and GGC-8-H200 were 1779  $\mu\epsilon$  and 1803  $\mu\epsilon$ , respectively, yielding  $\epsilon_{fg}/\epsilon_f$  ratios of 9.4% and 9.5%, respectively. The well-confined GGC-8-H50, on the other hand, yielded the highest  $\epsilon_{fg}$  among the columns with circular hoops, equivalent to 3070  $\mu\epsilon$  or 13.3% of  $\epsilon_f$ . GGC-8-S50 and GGC-8-S100 developed  $\epsilon_{fg}$  of 2116  $\mu\epsilon$  and 1967  $\mu\epsilon$ , respectively, translating to strain development of 11.2% and 10.4% of  $\epsilon_f$ , respectively. The strains in the bars at  $P_c$  load level were also summarized in Table 4. The  $\epsilon_{fc}$  were 6047  $\mu\epsilon$ , 5955  $\mu\epsilon$ , 8648  $\mu\epsilon$ , and 7866  $\mu\epsilon$  for GGC-8-H50, GGC-8-H100, GGC-8-S50, and GGC-8-S100, respectively, translating to  $\epsilon_{fc}/\epsilon_f$  ratios of 32.0%, 31.5%, 45.8%, and 41.6%, respectively. These values were lower than the strain ratio capacity (51.7%) reported earlier. GGC-16-H100 (1436  $\mu\epsilon$ ) and GGC-16-S100 (1922  $\mu\epsilon$ ) produced  $\epsilon_{fg}/\epsilon_f$  ratios of 7.6% and 10.2%, respectively. These results showed that the GFRP bars had a compression contribution that cannot be neglected. Interestingly, the average

$\epsilon_{fg}$  of the short columns  $\epsilon_{fg-av}$  (2036  $\mu\epsilon$ ) was relatively comparable to  $\epsilon_{cg-ave}$ , suggesting the compatibility between the bars and the geopolymer concrete and that equivalency between these materials could be assumed for design and analysis purposes. Furthermore, this strain value was higher than the design strain limit of 1000  $\mu\epsilon$  proposed by Zadeh and Nanni [55] to avoid exaggerated deflections.

Figure 13 shows the relationships between the axial load and the lateral-tie strain. Marginal strains ( $\epsilon_{ftg}$ ) were recorded at lower loads. After exceeding the load equivalent to GGC-8-H100's  $P_g$ , however, relatively higher strains were obtained from GGC-8-H50 and GGC-8-S50 because of the early spalling of their concrete covers compared to the columns with wider tie spacing. The  $\epsilon_{ftg}$  of GGC-8-H50 (1729  $\mu\epsilon$ ) was higher than that of GGC-8-H100 (664  $\mu\epsilon$ ) and GGC-8-H200 (853  $\mu\epsilon$ ). A similar trend was also observed in the spiral-confined columns with GGC-8-S50 (968  $\mu\epsilon$ ) yielding a higher  $\epsilon_{ftg}$  than GGC-8-S100 (730  $\mu\epsilon$ ). The trend reversed, however, right after the  $P_g$  load level was reached. The  $\epsilon_{ftc}$ , the transverse reinforcement strain at  $P_c$  load level, were 5569  $\mu\epsilon$  and 13131  $\mu\epsilon$  for GGC-8-H100 and GGC-8-S100, respectively. These strains were higher than that of GGC-8-H100 (3302  $\mu\epsilon$ ) and GGC-8-S100 (7765  $\mu\epsilon$ ), respectively. On the other hand, the columns with spiral reinforcement generally yielded higher  $\epsilon_{ftc}$  compared to their counterpart columns with circular hoops. GGC-16-H100 and GGC-16-S100 recorded  $\epsilon_{ftg}$  values of 552  $\mu\epsilon$  and 700  $\mu\epsilon$ , respectively, which were lower than their counterpart short columns.

**Table 4**  
Geopolymer concrete and GFRP reinforcement strains.

Column	$\epsilon_{cg}$ , $\mu\epsilon$	$\epsilon_{fg}$ , $\mu\epsilon$	$\epsilon_{fc}$ , $\mu\epsilon$	$\epsilon_{ftg}$ , $\mu\epsilon$	$\epsilon_{ftc}$ , $\mu\epsilon$
GGC-8-00	1424	1647	-	-	-
GGC-8-H50	2129	2518	6047	1729	3302
GGC-8-H100	1845	1779	5955	664	5569
GGC-8-H200	2183	1803	-	853	-
GGC-8-S50	2183	2116	8680	968	7765
GGC-8-S100	1821	1967	7866	730	13131
GGC-16-H100	1266	1436	-	552	-
GGC-16-S100	637	1922	-	700	-

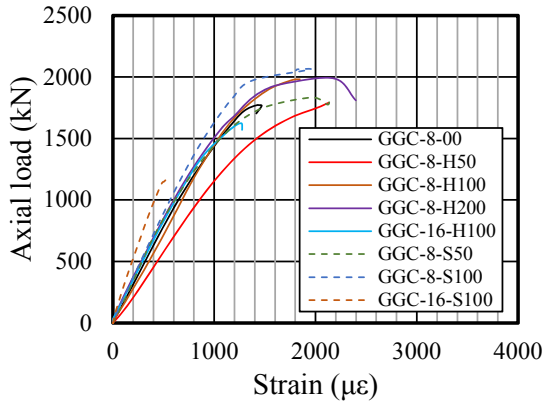


**Fig. 11.** Axial load versus geopolymer concrete strain curves.

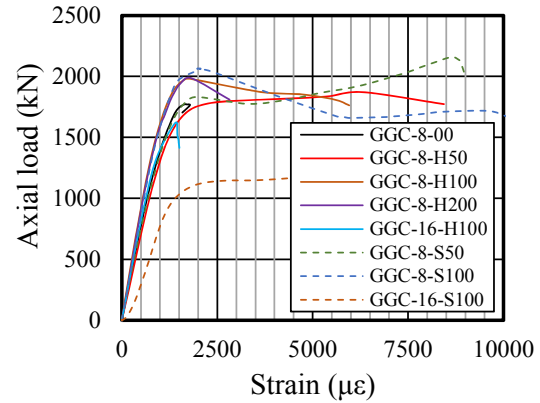


**Fig. 12.** Axial load versus longitudinal bar strain curves.

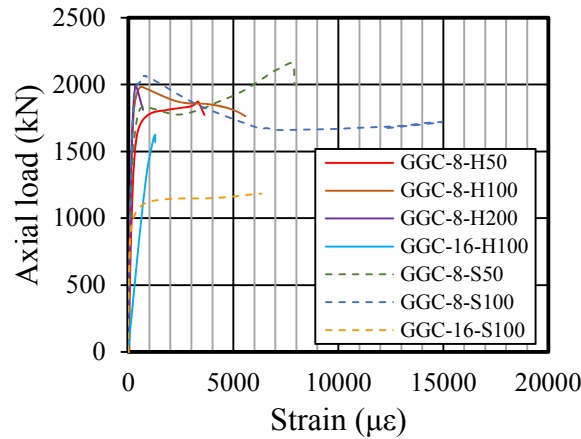


**Fig. 13.** Axial load versus lateral-tie strain curves.

### 3.5. Confinement Efficiency and Ductility Index

In this study, the column ductility index (D.I.) was defined as the ratio of the displacement that corresponds to 85% of  $P_{peak}$  to the displacement that corresponds to the elastic behavior limit ( $\Delta_{85}/\Delta_1$ ), as shown in Figure 14. The procedure for determining these displacements was based on Pantelides et al.'s [26] recommendations. The confinement efficiency (C.E.), on the other hand, was computed as the ratio of the compressive strength of the confined column to the compressive strength of the unconfined column ( $f'_{cc}/f'_{co}$ ). The  $f'_{cc}$  was calculated as the peak load divided by the area of the confined geopolymer concrete, which is represented by point C

in Figure 15. The  $f'_{co}$ , on the other hand, was equivalent to  $0.90f'_c$ . Table 5 summarizes the D.I. and C.E. values of the tested columns. Based on the experimental results, the ductility index and confinement efficiency increased when the amount of transverse reinforcement increased. These results are consistent with Afifi et al.'s [39] findings on circular concrete columns reinforced with GFRP bars and spirals. Sharma et al. [58] also reported a similar trend regarding the ductility of the confined columns for conventional RC columns. The geopolymer concrete columns with spiral reinforcement, in general, showed higher ductility and confinement efficiency than those with circular hoops. These findings are not consistent with those of Mohamed et al. [40] wherein they concluded that the FRP circular hoops have similar confining efficiency as the FRP spirals. This could be expected since they utilized hoops with longer lap or splice lengths, approximately 2.5 to 5 times longer than that of the hoops employed in this study. The ductility and confinement efficiency of the slender geopolymer concrete columns were not considered in this study, mainly because of the nature of failure of these specimens.

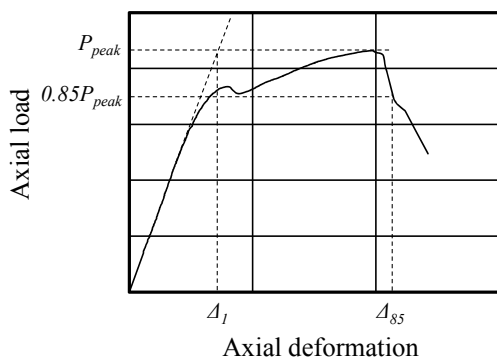


**Fig. 14.** Definition of  $\Delta_{85}$  and  $\Delta_1$ .

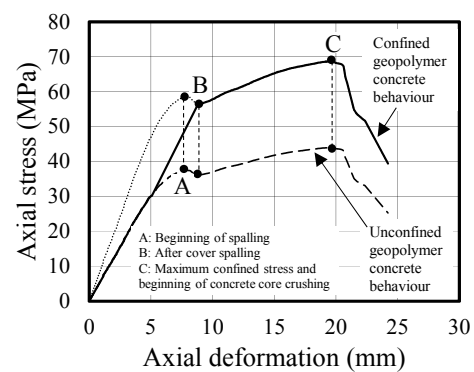


**Fig. 15.** Confined stress-deformation curve of GGC-8-S50.



**Table 5**

Normalised strength, ductility index (D.I.) and confinement efficiency (C.E.) of GFRP-RGC and GFRP-RC circular columns.

Author	Specimen	Type	$\rho_{ft}$ (%)	$\frac{P_g - P_{fg}}{f'_c A_g}$	D.I.	C.E.
Current Study	GGC-8-H50	Hoop	3.13	85.9	2.08	1.84
	GGC-8-H100	Hoop	1.57	99.1	1.32	1.74
	GGC-8-S50	Spiral	3.13	90.1	2.99	2.13
	GGC-8-S100	Spiral	1.57	102.7	1.79	1.67
Afifi et al. 2013	G4V-3H80	Spiral	1.48	89.0	1.13	1.37
	G8V-3H40	Spiral	2.95	89.4	4.75	1.89
	G8V-3H80	Spiral	1.48	89.2	2.00	1.69
	G8V-3H120	Spiral	0.98	85.9	1.54	1.32
	G12V-3H80	Spiral	1.48	89.4	2.45	1.78
Mohamed et al. 2014	G3H200	Hoop	1.48	88.8	1.83	1.57
	G3H400	Hoop	1.48	84.8	1.88	1.60
	G3H600	Hoop	1.48	87.7	1.91	1.63
Pantelides et al. 2013	13GLCTL	Spiral	1.91	-	1.70	1.76
	14GLCTL	Spiral	1.91	-	3.60	1.59

### 3.6. Lateral Deflection

Figure 16 shows the typical lateral deflection readings, just before the initiation of concrete-cover spalling, obtained from the horizontally positioned laser displacement sensors. The black lines represent that of the short columns while the red and green lines correspond to that of GGC-16-H100 and GGC-16-S100. At lower applied loads, the deflection was approximately equivalent to zero for both column types. At higher loads, however, the GGC-8 columns yielded relatively random readings owing to the geopolymer-concrete crushing and cracking. The slender columns, on the other hand, yielded deflections that increased hyperbolically with increasing loads, clearly indicating that the columns were undergoing lateral buckling.

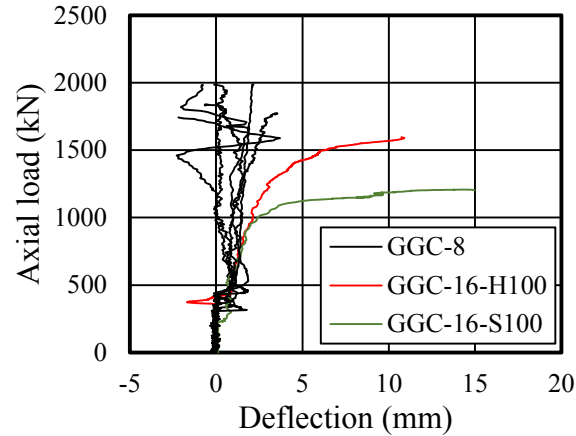


**Fig. 16.** Axial load versus lateral deflection.

## 4. Discussion

### 4.1. Influence of the Transverse Reinforcement

The provision of transverse reinforcement generally enhanced the compression performance of the tested GFRP-RGC columns. The compression failure of the confined columns was less brittle compared to the unconfined control specimen. At  $P_g$  load level, the average strength and deformation capacity of the confined columns were 10% and 1%, respectively, higher than that of the corresponding values for the unconfined column. Furthermore, the average geopolymer concrete and longitudinal GFRP bar strains of confined columns were 24% and 43% higher, respectively, than that of the unconfined column, suggesting the ties' effectiveness in enhancing the strain development in each component material of the column.

### 4.2. Influence of the Transverse-Reinforcement Spacing

The effect of the amount of transverse reinforcement on the performance of confined concrete has been well studied. As can be expected, the closer the tie spacing or the larger the volumetric ratio, the less brittle the compression failure of the tested columns, showing a slower rate of strength decay after the peak. After the geopolymer-concrete cover spalled, the well-confined

columns (GGC-8-H50 and GGC-8-S50) showed relatively higher strength and deformation capacities than the less-confined columns (GGC-8-H100 and GGC-8-S100). These observations tend to support Paultre and Legeron's [59] generalization for confined columns, which states that the effectiveness of confinement reinforcement in restraining concrete varies from "one" for a continuous tube to "zero" when the ties are spaced more than half the minimum core cross section. This conclusion may also explain why the poorly confined GGC-8-200 evidenced load–deformation behavior and failure mode similar to GGC-8-00, since the hoop spacing was too wide to provide any lateral confinement. Interestingly, the columns with a volumetric ratio of 3.13% or a transverse-reinforcement spacing of 50 mm on centers yielded another peak and deformation capacities that were higher than their initial capacities. This can be related to the high confinement that enhanced the geopolymer-concrete core and prevented vertical GFRP bar buckling, owing to reduced the unbraced length of the bars, which enhanced the compression contribution of the GFRP bars.

The amount of transverse reinforcement, expressed in terms of  $\rho_{ft}$ , played a major role after the concrete cover spalled. An adequate amount of lateral reinforcement with respect to the unsupported length of longitudinal reinforcement ensured the stability of the longitudinal reinforcement between the ties. Furthermore, after the concrete spalled, the well-confined geopolymer-concrete columns yielded an ascending load–deformation relationship, while the poorly confined geopolymer-concrete columns produced a descending response.

#### ***4.3. Influence of the Transverse-Reinforcement Configuration***

The geopolymer-concrete columns confined by spirals exhibited relatively higher ductility and confinement efficiency compared to their counterpart columns confined with circular hoops, owing to the continuous nature of the spirals, which effectively confined the whole geopolymer-concrete core by distributing the lateral confining pressures uniformly around the

perimeter and along the height of the geopolymer-concrete core. This observation corroborates Yong et al.'s [60] and Mohamed et al.'s [40] findings for conventional RC and FRP-RC columns, respectively. Furthermore, the difference between the two types of lateral ties can be clearly seen after the spalling of the concrete cover of the well-confined columns. The  $P_c$ -to- $P_g$  ratio of GGC-8-S50 was 1.18, whereas, for GGC-8-H50, the ratio was just 1.04. This result tends to suggest that the strength enhancement in hoop-confined columns due to transverse reinforcement could be ignored. Interestingly, this finding corroborates those of Kent and Park [61] for rectangular conventional RC columns transversely reinforced with rectilinear ties, in which the concrete core delineated by the outer tie diameter was not fully confined due to the non-uniform lateral pressure that resulted in poor strength enhancement. This could be attributed to the discontinuous nature of the circular hoops, since the column failure was governed by lap-splice failure at the joint and not by the GFRP ties rupturing. It can be deduced, therefore, with the same amount of strength and ductility improvement, hoop-confined columns should be much more confined than spiral-confined columns.

#### ***4.4. Influence of the Slenderness Ratio ( $L/r$ )***

Generally, the columns with higher slenderness ratios and confined with hoops and spirals yielded strength capacities ( $P_g$ ) that were 66% and 82% of the strength of their short-column counterparts. The hoop-confined slender column yielded  $\epsilon_{cg}$ ,  $\epsilon_{fg}$ , and  $\epsilon_{ftg}$  that were just 35%, 80%, and 83%, respectively, of the strains of their counterpart hoop-confined short columns. The spiral-confined slender column, on the other hand, recorded strains that were 68%, 97%, and 95%, respectively, of the corresponding values for spiral-confined short columns. Furthermore, the confinement efficiency of the hoop- and spiral-confined slender columns was just 59% and 46%, respectively, of their counterpart short columns. These results could be attributed to the buckling failure of the slender columns—a geometric type of failure not related

to the strength of the material—which lowered their strength capacities and did not allow the efficient use of each component material. The higher deformation values could be attributed to column lateral movement. Clearly, these results indicate the influence of slenderness in the tested columns with  $L/r=16$ , thereby suggesting that the previously proposed slenderness limit for GFRP-RC columns (17.2) must be lowered for the proposed system. The critical buckling load  $P_c$ —estimated from Equation 1—was equivalent to 1898 kN. This is higher than the  $P_g$  of the tested slender columns, indicating that a lower  $P_c$  limit must be adopted for the proposed system. Further research is needed, however, to support these generalizations.

$$P_c = \frac{\pi^2 EI}{(kL_u)^2} \quad (1a)$$

$$EI = \frac{0.2E_c I_g + E_f I_{se}}{(1 + \beta_d)} \quad (1b)$$

#### 4.5. Theoretical Prediction

The nominal capacities of the tested GFRP-RGC columns were determined using the equations below. These formulas were used to estimate column strength at  $P_g$  load levels. Figure 17 shows the comparison of the experimental-to-predicted ( $P_g$ -to- $P_o$ ) ratios using these equations.

$$P_o = \alpha_1 f'_c (A_g - A_f); \alpha_1 = 0.85 - 0.0015 f'_c \geq 0.67 \quad (2)$$

$$P_o = 0.85 f'_c (A_g - A_f) \quad (3)$$

$$P_o = 0.85 f'_c (A_g - A_f) + \alpha_g f_{fu} A_f \quad (4)$$

$$P_o = 0.90 f'_c (A_g - A_f) + \epsilon_{fg} E_f A_f \quad (5)$$

Of the current North American standards for FRP-RC systems, only CSA S806-12 has established a prediction equation for FRP-RC columns, as depicted by Equation 2. This equation, however, ignores the compression contribution of the FRP bars. Using this equation, the ratios of the peak experimental load-to-predicted nominal capacity ( $P_g/P_o$ ) varied from 113% to 143%, with an average value of 129%. Equation 3 was based on the equation in ACI 318-11 [62] recommended for conventional RC columns. It neglects, however, the compression contribution of GFRP bars. Based on this formula, the  $P_g/P_o$  ratios ranged from 105% to 129% with an average value of 121%, yielding less conservative estimates compared to Equation 1.

Equation 4 depicts the equation recommended by Afifi et al. [39]. The compression contribution of the GFRP bars was considered by introducing a factor  $\alpha_g$  that accounts for the reduced compressive strength of the GFRP bars as a function of their tensile strength. Currently, no standard test is available to determine the compressive strength of FRP bars. Hence, in order to determine the factor  $\alpha_g$  in this study, five 15.9 mm GFRP bars 40 mm in length were used and were subjected to compressive testing. The test yielded an average  $\alpha_g$  approximately equivalent to 0.5. From Equation 4, the  $P_g/P_o$  ratios ranged from 72% to 92% and an average of 83%. This equation generally yielded unconservative estimates, indicating its inapplicability for the proposed system. Equation 5 was based on Mohamed et al.'s [40] recommendations, although we used a reduction factor of 0.90 obtained from the experiment instead of the commonly used value of 0.85. Adoption of higher strength-reduction factor seems to be logical for the proposed system owing to the higher elastic modulus of the geopolymer concrete (33 GPa) compared to a normal concrete (29 GPa, calculated using the ACI 318-11 formula) of the same grade (38 MPa). This would result in better compatibility in the GFRP-RGC system, as evidenced by the recorded average strains in the GFRP bars and geopolymer concrete that, subsequently, would yield more area under the stress-strain curve

compared to a GFRP-RC system. Further studies, however, are recommended to validate these conclusions. The longitudinal reinforcement's contribution was calculated based on the actual strains in the bars, represented by  $\varepsilon_{fg-ave}$ . This strain corresponds to the average compression strain in GFRP bars at the  $P_g$  load level or the strain at which the plastic deformation of the geopolymer concrete initiated. Based on the column compression test, the  $\varepsilon_{fg-ave}$  was equivalent to 0.002. The  $P_g/P_o$  ratios varied from 68% to 111%, with an average value of 100%. Interestingly, among the equations considered herein, this equation yielded the relatively most accurate prediction of the nominal capacity of the column specimens. In addition, this equation produced conservative estimates, except for the slender columns, thereby suggesting the equation's suitability in predicting the capacity of short GFRP-RGC columns. A new equation must, therefore, be proposed to consider the slenderness effect on the capacity of GFRP-RGC columns.

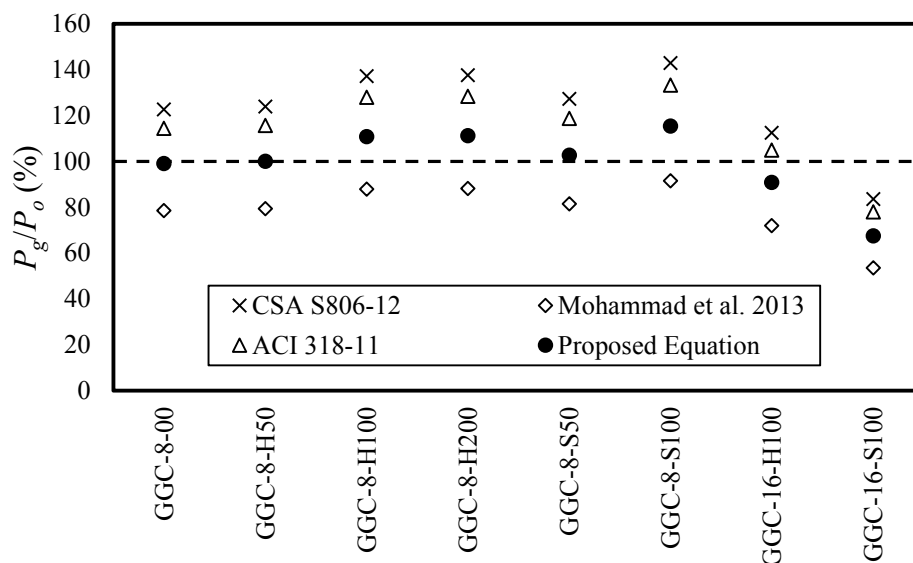


**Fig. 17.**  $P_g$ -to- $P_o$  ratios.

#### 4.6. Comparison with the GFRP-RC Circular Columns

The performance of the tested GFRP-RGC circular columns was compared to that of Afifi et al.'s [39], Mohamed et al.'s [40], and Pantelides et al.'s [26] GFRP-RC circular columns in terms of normalized strength, ductility index, and confinement efficiency. These values were

summarized in Table 5. The normalized strength was calculated as the difference between  $P_g$  and  $P_f$  divided by the concrete strength ( $f'_c$ ) and the gross area ( $A_g$ ) of the column. From the table, it can be seen that the strength of the GFRP-RGC columns were higher than that of the GFRP-RC columns. Interestingly, this finding tends to support the authors' earlier claim that GFRP bars have better compatibility with geopolymer concrete compared with OPC concrete, owing to the higher elastic modulus of the former concrete compared to the latter concrete. Comparing the ductility and confinement efficiency of GFRP-RGC columns to that of GFRP-RC columns with comparable amounts and types of transverse reinforcement, the two systems showed relatively comparable performance. From these findings, it can be inferred that GFRP bars can be used as reinforcement for geopolymer-concrete columns, particularly when structural columns that are corrosion resistant and electromagnetic transparent are targeted. This conclusion corroborates Zadeh and Nanni's [55] generalization based on past experimental research, stating that GFRP bars can be used to strengthen conventional RC columns.

#### ***4.7. Proposed stress-strain model for GFRP-RGC Circular Columns***

Figure 18 shows the stress-strain curve adopted in this study. The linear elastic segment represents that of the unconfined and confined behaviour while the remaining segment embodies that of the confined behaviour only, upon the activation of the GFRP ties' passive confinement. Equations 6a-e, proposed by Popovics [63], was employed to model the ascending branch (O-A-B) while Equations 7a-c, which was proposed by Han et al. [64] for high strength reinforced concrete tied columns, was used to model the descending part (B-C-D). The maximum confining pressure ( $f_{IGFRP}$ ) was computed from Equation 8a-b. The constants  $a, b, c, d, e, f, g, h, i,$  and  $j$  were determined through the regression analysis of short columns' experimental results, as implemented by Han et al. [64], such as the confined compressive strength ( $f'_{cc}$ ); the axial strains, derived from longitudinal reinforcement strains, at  $f'_{cc}, 0.85f'_{cc}$ ,



and  $0.50 f'_{cc}$  ( $\varepsilon_{cc}$ ,  $\varepsilon_{0.85cc}$ , and  $\varepsilon_{0.50cc}$ , respectively); and transverse reinforcement strain at  $f'_{cc}$  ( $\varepsilon_{ftcc}$ ). These constants were tabulated in Table 6. Figure 19 shows a good correlation between the predicted and the experimental stress-strain curves for the tested GFRP-RGC column specimens. The proposed equations, however, are applicable only for the specimens considered in this study. Further research works are needed to further calibrate the proposed equations.

$$f_c = \frac{f'_{cc} (\varepsilon_c / \varepsilon_{cc})^m}{m-1 + (\varepsilon_c / \varepsilon_{cc})^m}, \varepsilon_c \leq \varepsilon_{cc} \quad (6a)$$

$$m = \frac{E_c}{E_c - E_{sec}} \quad (6b)$$

$$E_{sec} = f'_{cc} / \varepsilon_{cc} \quad (6c)$$

$$f'_{cc} = f'_{co} + a (\rho_{ft} f_{IGFRP})^b \quad (6d)$$

$$\varepsilon_{cc} = \varepsilon_{co} \left[ 1 + c \left( \frac{\rho_{ft} f_{IGFRP}}{f'_{co}} \right)^d \right] \quad (6e)$$

$$f_c = f'_{cc} \left[ 0.85 - 0.5 \frac{\varepsilon_c - \varepsilon_{0.85cc}}{\varepsilon_{0.50cc} - \varepsilon_{cc}} \right] \geq 0.3 f'_{cc} \quad (7a)$$

$$\varepsilon_{0.85cc} = \varepsilon_{co} \left[ 1 + e \left( \frac{\rho_{ft} f_{IGFRP}}{f'_{co}} \right)^f \right] \quad (7b)$$

$$\varepsilon_{0.50cc} = \varepsilon_{co} \left[ 1 + g \left( \frac{\rho_{ft} f_{IGFRP}}{f'_{co}} \right)^h \right] \quad (7c)$$

$$f_{IGFRP} = \frac{\rho_{ft}}{2} E_f \varepsilon_{ftcc} \quad (8a)$$

$$\varepsilon_{ftcc} = i \times \exp \left[ j (\varepsilon_{ft} / s) \right] \quad (8b)$$

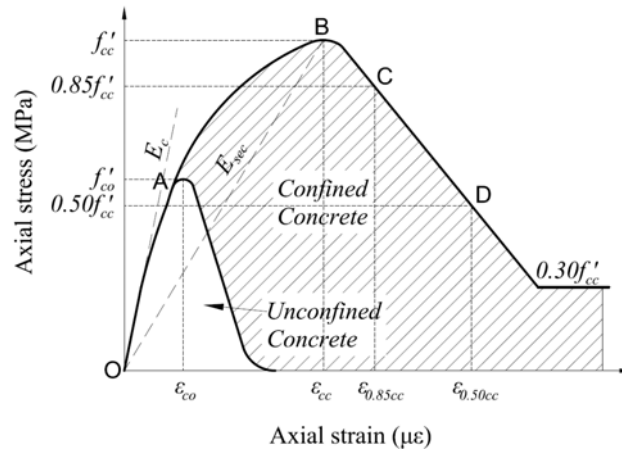


**Fig. 18.** Adopted stress-strain curve for the confined geopolymer concrete.

**Table 6**  
Constants  $a, b, c, d, e, f, g, h, i,$  and  $j$ .

Column	$a$	$b$	$c$	$d$	$e$	$f$	$g$	$h$	$i$	$j$
Hoop-confined column	22.01	-0.03	72.23	0.54	102.4 0	0.40	210.54	0.36	790.1	0.003
Spiral-confined column	34.88	0.05	132.8 8	0.64	35.39	0.36	7.25	0.02	196.1	0.009

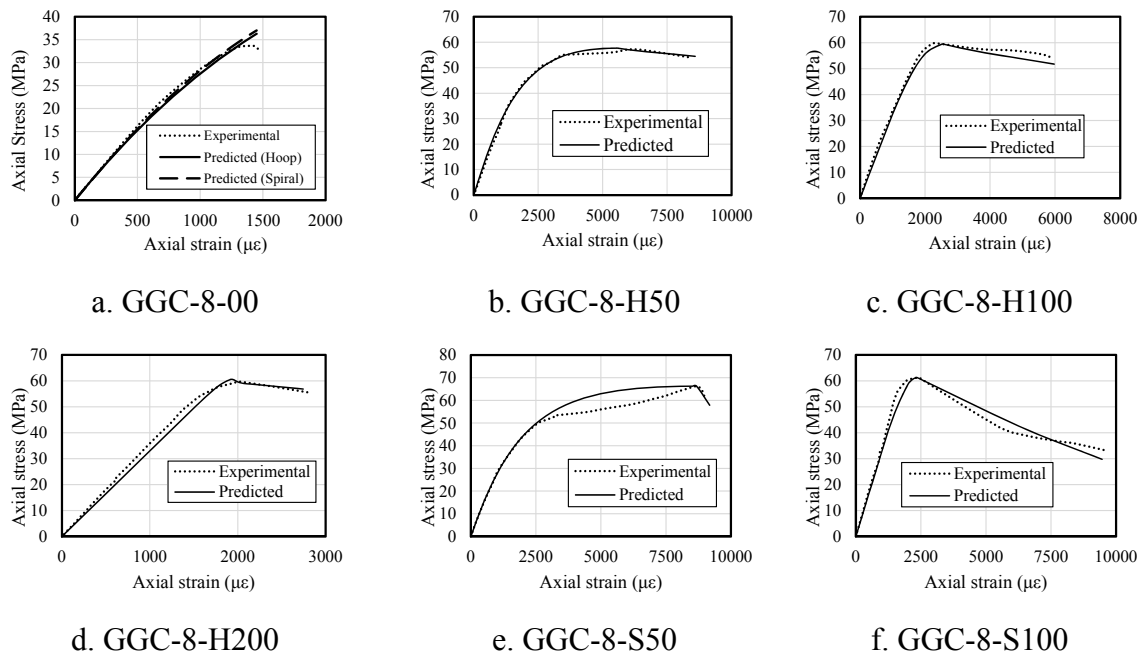


**Fig. 19.** Experimental and predicted stress-strain curves of the GFRP-RGC columns.

#### 4.8. Proposed compression relationship for GFRP bars

It was evident from the experiment that the GFRP bars in the columns with ties spaced at 50-200 mm exhibited local combined crushing and buckling failure while the control specimen undergone buckling failure; hence, two equations were proposed. Equation 9a shows the proposed relationship for predicting the ultimate compression stress in the GFRP bars ( $f'_{fu}$ ) that undergone local combined crushing and buckling failure. The maximum value of 612.5 MPa was adopted from the compression test of GFRP bars. This equation was basically derived from the regression analysis of the experimental results acquired from the actual column test. To calculate the experimental  $f'_{fu}$ , the load  $P_{fg}$  was divided by the total area and number of longitudinal bars. The compression behaviour of GFRP bars encased in geopolymer concrete and confined by a closely spaced ties can intuitively be expected to be different from that of buckling test of the bars. The buckling test resulted in a fixed-fixed end condition while in the column test, the end conditions are not as simply defined. Furthermore, buckling behaviour of GFRP bars is not only influenced by the lateral bracing distance (or tie spacing) but also by the geopolymer concrete core condition [65]. Equation 9b, on the other hand, predicts that of GFRP bars that undergone global buckling failure, the bars in the control specimen. Interestingly, the obtained effective length factor  $k$  (0.926) was approximately equivalent to 1.0, which is typically adopted for pinned-end specimen. Table 7 shows a good agreement between the experimental and predicted results. Further research works, however, are needed to enhance the accuracy the proposed equations.

$$f'_{fu} = 612.5 - 53.564 \times s \times \left( \frac{L_{uf}}{r_f} \right)^{-0.946} \quad \text{For: } 50 \text{ mm} \leq L_{uf} \leq 200 \text{ mm} \quad (9a)$$

$$f'_{fu} = \frac{\pi^2 E_{fc}}{(kL_{uf}/r_f)^2}; k = 0.926 \quad \text{For: } L_{uf} > 200 \text{ mm} \quad (9b)$$

**Table 7**

Compressive stress in GFRP bars.

Column	$L_{uf}$ , mm	<i>Experimental</i> , MPa	<i>Predicted</i> , MPa
GGC-8-00	667	102	101.5
GGC-8-H50	50	158	142.2
GGC-8-H100	100	112	124.3
GGC-8-H200	200	112	105.7
GGC-8-S50	50	133	142.2
GGC-8-S100	100	123	124.3

## 5. Conclusion

This study investigated the behavior of geopolymer-concrete columns reinforced longitudinally and transversely with GFRP bars. From the experimental results, the following conclusions were drawn:

- The compression contribution of the GFRP bars (2.43% reinforcement ratio) with respect to column capacity prior to concrete spalling varied from 6.6% to 10.5%, with an average value of 7.6%.
- Irrespective of tie configuration, the columns with closely spaced lateral ties or higher volumetric ratios failed in a more ductile manner and showed higher confinement efficiency compared to the columns with relatively lower volumetric ratios. The hoop- and spiral-confined columns with ties spaced at 50 mm on centers yielded ductility indices [confinement efficiency] that were 58% [7%] and 67% [28%], respectively, higher than their counterpart columns with ties spaced 100 mm on centers.
- The spiral-confined columns exhibited a more ductile behavior and higher post-concrete-cover spalling strength compared to their hoop-confined counterparts, as proven by the higher average ductility index and average confinement efficiency (2.39 and 1.90, respectively) of the spiral-confined columns compared to the hoop-confined

ones (1.79 and 1.70, respectively). These findings could be attributed to the uniform lateral confining pressure of the spirals.

- The short columns failed due to crushing and/or shear failure, while the slender columns failed due to buckling. Hence, irrespective of the type and amount of transverse reinforcement, the short columns yielded higher compression capacities than the slender columns. The hoop- and spiral-confined short columns with ties spaced at 100 mm on centers yielded strength capacities that were 22% and 71%, respectively, higher than their counterpart slender columns.
- The GFRP-RGC circular columns yielded a relatively higher normalized strength (97.3%) compared to GFRP-RC circular columns (88.3%). This could be attributed to the higher elastic modulus of geopolymer concrete (33 GPa) compared to normal concrete (29 GPa) of the same grade (38 MPa), resulting in better compatibility in the GFRP-RGC system than in a GFRP-RC system. Further studies, however, are needed to validate this generalization.
- The slender columns failed at a load 66% and 82% of the strength of their short-column counterparts. They exhibited higher deformation compared to the short columns due to the lateral movement and they failed due to buckling.
- The nominal capacity of the tested columns could be estimated accurately using the proposed equation because it considers the actual geopolymer-concrete strength-reduction factor (0.90) and the actual compression contribution of the GFRP bars (using the average bar strain as being equivalent to 2000  $\mu\epsilon$ ).
- The proposed confined stress-strain equations show good correlation with the experimentally established stress-strain relationship for the GFRP-RGC columns. Further research works, however, are needed to further calibrate these equations.

- It can be inferred, therefore, that a GFRP-RGC system could be adopted as compression members, particularly when corrosion resistance, electromagnetic transparency, material greenness, durability, and sustainability are sought.

### Nomenclature:

$A_b$	= nominal area of the GFRP bars ( $\text{mm}^2$ )
$A_f$	= total area of the longitudinal GFRP reinforcement ( $\text{mm}^2$ )
$A_g$	= gross cross-sectional area of the column ( $\text{mm}^2$ )
$A_{ft}$	= cross-sectional area of the transverse reinforcement ( $\text{mm}^2$ )
$D$	= column diameter (mm)
$D_c$	= concrete-core diameter delineated by the outside diameter of hoops or spirals (mm)
$E_c$	= modulus of elasticity of the concrete (MPa)
$E_f$	= tensile modulus of the GFRP bars (MPa)
$E'_f$	= compression modulus of the GFRP bars (MPa)
$E_{sec}$	= tangent modulus modulus of elasticity of the concrete (MPa)
$EI$	= flexural stiffness of the reinforced-concrete column
$f_{fu}$	= tensile strength of the GFRP bars (MPa)
$f'_{fu}$	= ultimate compressive stress in the GFRP bars (MPa)
$f'_c$	= concrete compressive strength (MPa)
$f'_{cc}$	= confined-column compressive strength (MPa)
$f'_{co}$	= unconfined-column in-place compressive strength, $0.9f'_c$ (MPa)
$f'_{IGFRP}$	= maximum confinement pressure
$I_{se}$	= moment of inertia of reinforcement about members' centroidal axis ( $\text{mm}^4$ )
$k$	= effective length factor for buckling
$k_a$	= efficiency factor that accounts for the geometry of the section, taken as 1.0 for circular sections
$k_e$	= efficiency factor that accounts for the premature failure of the FRP system
$L$	= column height (mm)
$L/r$	= slenderness ratio
$L_{uf}$	= unsupported length of GFRP bars (mm)
$m$	= parameter that controls the initial slope and curvature of the ascending branch
$n$	= number of longitudinal bars
$P_c$	= concrete core capacity (N, kN)
$P_{fc}$	= compression contribution of GFRP bars at $P_c$ load level (N, kN)
$P_{fg}$	= compression contribution of GFRP bars at $P_g$ load level (N, kN)
$P_g$	= gross capacity of the column (N, kN)
$P_o$	= nominal capacity of the column (N, kN)
$P_{peak}$	= peak capacity of the column (N, kN)
$r$	= radius of gyration (mm)
$r_f$	= radius of gyration of GFRP bars (mm)
$s$	= circular hoop spacing or spiral pitch on-center (mm)
$\alpha_g$	= compressive-strength reduction of the GFRP bar as a function of its tensile strength
$\beta_d$	= concrete creep factor (assumed equivalent to 1.0 in this study)
$\Delta_c$	= deformation at $P_c$ load level (mm)
$\Delta_g$	= deformation at $P_g$ load level (mm)

$\Delta l$	= displacement that corresponds to the limit of the elastic behavior (mm)
$\Delta_{85}$	= displacement that corresponds to 85% of maximum load (mm)
$\varepsilon_c$	= axial strain in geopolymer concrete ( $\mu\varepsilon$ )
$\varepsilon_{cc}$	= axial strain in confined geopolymer concrete at $f'_{cc}$ ( $\mu\varepsilon$ )
$\varepsilon_{0.50cc}$	= axial strain in confined geopolymer concrete at $0.50f'_{cc}$ ( $\mu\varepsilon$ ) in the descending branch of the stress-strain model
$\varepsilon_{0.85cc}$	= axial strain in confined geopolymer concrete at $0.85f'_{cc}$ ( $\mu\varepsilon$ ) in the descending branch of the stress-strain model
$\varepsilon_{cg}$	= average axial concrete strain at $P_g$ load level ( $\mu\varepsilon$ )
$\varepsilon_{cg-ave}$	= average of $\varepsilon_{cg}$ ( $\mu\varepsilon$ )
$\varepsilon_{co}$	= axial strain in unconfined geopolymer concrete corresponding to $f'_{co}$ ( $\mu\varepsilon$ )
$\varepsilon_f$	= ultimate tensile strain of the GFRP bars
$\varepsilon_{fc}$	= average strain in the longitudinal GFRP bars at $P_c$ load level ( $\mu\varepsilon$ )
$\varepsilon_{fg}$	= average strain in the longitudinal GFRP bars at $P_g$ load level ( $\mu\varepsilon$ )
$\varepsilon_{fg-ave}$	= average of $\varepsilon_{fg}$ ( $\mu\varepsilon$ )
$\varepsilon_{ftg}$	= average tie strain at $P_g$ load level ( $\mu\varepsilon$ )
$\varepsilon_{ftc}$	= average tie strain at $P_c$ load level ( $\mu\varepsilon$ )
$\varepsilon_{ftcc}$	= tie strain at $f'_{cc}$ ( $\mu\varepsilon$ )
$\varepsilon_{ft}$	= ultimate tensile strain of the transverse reinforcement ( $\mu\varepsilon$ )
$\gamma_b$	= safety factor
$\mu$	= ductility index
$\phi_f$	= nominal diameter of the GFRP bars (mm)
$\rho_f$	= longitudinal reinforcement ratio
$\rho_{ft}$	= transverse reinforcement volumetric ratio

## Acknowledgement

The authors would like to express their special thanks to V-ROD® Australia for providing the materials as well as to the Natural Science and Engineering Research Council of Canada (NSERC) and the technical staff of the structural lab at University of Southern Queensland.

## References

- [1] Rizkalla S, Hassan T, Hassan N. Design recommendations for the use of FRP for reinforcement and strengthening of concrete structures. *Progress in Structural Engineering and Materials*. 2003;5:16-28.
- [2] Benmokrane B, El-Salakawy E, El-Ragaby A, Lackey T. Designing and testing of concrete bridge decks reinforced with glass FRP bars. *Journal of Bridge Engineering*. 2006.

- [3] Gangarao HVS, Tally N, Vijay PV. Reinforced concrete design with FRP composites: CRC Press; 2007.
- [4] Kong DLY, Sanjayan JG. Effect of elevated temperatures on geopolymer paste, mortar and concrete. *Cement and Concrete Research*. 2010;40:334-9.
- [5] Neupane K, Bajewa D, Shrestha R, Chalmers D, Sleep P. Mechanical properties of geopolymer concrete: Applicability of relationship defined by AS 3600. *Concrete in Australia*. 2014;40:50-6.
- [6] Davidovits J. Geopolymers: Inorganic polymeric new materials. *Journal of Thermal Analysis*. 1991;37:1633-56.
- [7] Duxson P, Provis JL, Lukey GC, Van Deventer JS. The role of inorganic polymer technology in the development of 'green concrete'. *Cement and Concrete Research*. 2007;37:1590-7.
- [8] Sofi M, van Deventer JSJ, Mendis PA, Lukey GC. Engineering properties of inorganic polymer concretes (IPCs). *Cement and Concrete Research*. 2007;37:251-7.
- [9] Sarker PK. A constitutive model for fly ash-based geopolymer concrete. *Architecture Civil Engineering Environment (The Silesian University of Technology)*. 2008;1:113-20.
- [10] Olivia M, Nikraz H. Properties of fly ash geopolymer concrete designed by Taguchi method. *Materials and Design*. 2012;36:191-8.
- [11] Adam MA, Said M, Mahmoud AA, Shanour AS. Analytical and experimental flexural behavior of concrete beams reinforced with glass fiber reinforced polymer bars. *Construction and Building Materials*. 2015;84:354-66.
- [12] El-Nemr A, Ahmed EA, Benmokrane B. Flexural behavior and serviceability of normal- and high-strength concrete beams reinforced with glass fiber-reinforced polymer bars. *ACI Structural Journal*. 2013;110:1077-88.



- [13] Kassem C, Farghaly AS, Benmokrane B. Evaluation of flexural behavior and serviceability performance of concrete beams reinforced with FRP bars. *ASCE Journal of Composites for Construction*. 2011;15:682-95.
- [14] Benmokrane B, Chaallal O, Masmoudi R. Flexural response of concrete beams reinforced with FRP bars. *ACI Structural Journal*. 1996;91:46-55.
- [15] Mohamed K, Farghaly AS, B.Benmokrane. Effect of web reinforcement in FRP-reinforced deep beams. In: *Proceedings of the 7th International Conference on FRP Composites in Civil Engineering (CICE 2014)*. Vancouver, Canada; 2014. p. 79.
- [16] Razaqpur AG, Spadea S. Shear strength of FRP reinforced concrete members with stirrups. *Journal of Composites for Construction*. 2015;19:04014025.
- [17] Oller E, Marí A, Bairán JM, Cladera A. Shear design of reinforced concrete beams with FRP longitudinal and transverse reinforcement. *Composites Part B: Engineering*. 2015;74:104-22.
- [18] Kumaravel S, Thirugnanasambandam S. Flexural behaviour of geopolymer concrete beams. *International Journal of Advanced Engineering Research and Studies*. 2013;3:4-6.
- [19] Abraham R, Raj S D, Abraham V. Strength and behaviour of geopolymer concrete beams. *International Journal of Innovative Research in Science, Engineering and Technology*. 2013;2:159-66.
- [20] Dattatreya JK, Rajamane NP, Sabitha D, Ambily PS, Nataraja MC. Flexural behaviour of reinforced geopolymer concrete beams. *International Journal of Civil and Structural Engineering*. 2011;2:138-59.
- [21] Chang EH. Shear and bond behaviour of reinforced fly ash-based geopolymer concrete beams [PhD Thesis]. Perth, Australia: Curtin University of Technology; 2009.

- [22] Ambily P, Madheswaran C, Lakshmanan N, Dattatreya J, Sathik S. Experimental studies on shear behaviour of reinforced geopolymer concrete thin webbed T-beams with and without fibres. *International Journal of Civil & Structural Engineering*. 2012;3:128-40.
- [23] Ng TS, Foster SJ. Shear strength of lightweight fibre reinforced geopolymer concrete composite beam. In: Fragomeni S, Venkatesan S, Lam NTK, Setunge S, editors. 21st Australasian Conference on the Mechanics and Structures of Materials. Victoria University, Melbourne, Australia: Taylor & Francis Group; 2010. p. 77-82.
- [24] Maranan G, Manalo A, Benmokrane B, Karunasena W, Mendis P. Evaluation of the flexural strength and serviceability of geopolymer concrete beams reinforced with glass-fibre-reinforced polymer (GFRP) bars. *Engineering Structures*. 2015;101:529-41.
- [25] Maranan G, Manalo A, Karunasena W, Benmokrane B, Mendis P. Comparison of the shear behaviour of geopolymer concrete beams with GFRP and steel transverse reinforcements. In: Wu Z, Wu G, Wang X, editors. The 12th International Symposium on Fiber Reinforced Polymers for Reinforced Concrete Structures (FRPRCS-12) & The 5th Asia-Pacific Conference on Fiber Reinforced Polymer in Structures (APFIS-2015). Nanjing, China; 2015. p. 169.
- [26] Pantelides CP, Gibbons ME, Reaveley LD. Axial load behavior of concrete columns confined with GFRP spirals. *Journal of Composites for Construction*. 2013;17:305-13.
- [27] De Luca A, Matta F, Nanni A. Behavior of full-scale glass fiber-reinforced polymer reinforced concrete columns under axial load. *ACI Structural Journal*. 2010;107.
- [28] ACI 440.1R-06. Guide for the design and construction of structural concrete reinforced with FRP bars. Farmington Hills, Michigan, USA: American Concrete Institute; 2006.
- [29] CSA S806-12. Design and construction of building components with fibre-reinforced polymers. Toronto, Canada: Canadian Standards Association; 2012.

- [30] Chaallal O, Benmokrane B. Physical and mechanical performance of an innovative glass-fiber-reinforced plastic rod for concrete and grouted anchorages. *Canadian Journal of Civil Engineering*. 1993;20:254-68.
- [31] Deitz D, Harik I, Gesund H. Physical properties of glass fiber reinforced polymer rebars in compression. *Journal of Composites for Construction*. 2003;7:363-6.
- [32] Kobayashi K, Fujisaki T. Compressive behavior of FRP reinforcement in non-prestressed concrete members. In: Taerwe L, editor. *Proceedings of the 2nd International RILEM Symposium (FRPRCS 2): Non-Metallic (FRP) Reinforcement for Concrete Structures*: CRC Press; 1995. p. 267-74.
- [33] Wu W-P. Thermomechanical properties of fiber reinforced plastic(FRP) bars. *Dissertation Abstracts International (USA)*. 1992;52:292.
- [34] Paramanatham NS. Investigation of the behavior of concrete columns reinforced with fiber reinforced plastic rebars [MS Thesis]. Texas, USA: Lamar University; 1993.
- [35] Alsayed S, Al-Salloum Y, Almusallam T, Amjad M. Concrete columns reinforced by glass fiber reinforced polymer rods. *ACI Special Publication*. 1999;188.
- [36] Tobbi H, Farghaly AS, Benmokrane B. Concrete columns reinforced longitudinally and transversally with glass fiber-reinforced polymer bars. *ACI Structural Journal*. 2012;109.
- [37] Tobbi H, Farghaly AS, Benmokrane B. Behavior of concentrically loaded fiber-reinforced polymer reinforced concrete columns with varying reinforcement types and ratios. *ACI Structural Journal*. 2014;111.
- [38] Tobbi H, Farghaly AS, Benmokrane B. Strength model for concrete columns reinforced with fiber-reinforced polymer bars and ties. *ACI Structural Journal*. 2014;111.
- [39] Afifi MZ, Mohamed HM, Benmokrane B. Axial capacity of circular concrete columns reinforced with GFRP bars and spirals. *Journal of Composites for Construction*. 2013.

- [40] Mohamed HM, Afifi MZ, Benmokrane B. Performance evaluation of concrete columns reinforced longitudinally with FRP Bars and confined with FRP hoops and spirals under axial load. *Journal of Bridge Engineering*. 2014;19:04014020.
- [41] Sumajouw D, Hardjito D, Wallah S, Rangan B. Fly ash-based geopolymer concrete: study of slender reinforced columns. *Journal of Materials Science*. 2007;42:3124-30.
- [42] Sumajouw D, Hardjito D, Wallah S, Rangan B. Behavior of geopolymer concrete columns under equal load eccentricities. *ACI Special Publication*. 2005;228:577-94.
- [43] Sarker PK. Analysis of geopolymer concrete columns. *Materials and structures*. 2009;42:715-24.
- [44] Sujatha T, Kannapiran K, Nagan S. Strength assessment of heat cured geopolymer concrete slender column. *Asian Journal of Civil Engineering*. 2012;13:635-46.
- [45] Maranan G, Manalo A, Karunasena K, Benmokrane B. Bond stress-slip behavior: case of GFRP bars in geopolymer concrete. *Journal of Materials in Civil Engineering*. 2014;27:04014116.
- [46] Maranan G, Manalo A, Karunasena W, Benmokrane B. Pullout behaviour of GFRP bars with anchor head in geopolymer concrete. *Composite Structures*. 2015;132:1113-21.
- [47] CSA S807-10. Specification for fibre-reinforced polymers. Toronto, Canada: Canadian Standards Association; 2010. p. 44.
- [48] ACI 440.3R-12. Guide test methods for fiber-reinforced polymers (FRPs) for reinforcing or strengthening concrete structures. B2-Test method for longitudinal tensile properties of FRP bars. Farmington Hills, MI, USA: American Concrete Institute; 2012.
- [49] ASTM C39/C39M-15a. Standard test method for compressive strength of cylindrical concrete specimens. West Conshohocken, Pennsylvania, USA: ASTM International; 2015.
- [50] ASTM C143/C143M-15. Standard test method for slump of hydraulic-cement concrete. West Conshohocken, Pennsylvania, USA: ASTM International; 2015.

- [51] ASTM C807-13. Standard test method for time of setting of hydraulic cement mortar by modified vicat needle. West Conshohocken, Pennsylvania, USA: ASTM International; 2013.
- [52] Aldred J, Day J. Is geopolymer concrete a suitable alternative to traditional concrete. 37th Conference on our World In Concrete and Structures. Singapore 2012.
- [53] Mirmiran A. Length Effects on FRP-Reinforced Concrete Columns. In: Saadatmanesh H, Ehsani MR, editors. The 2nd International Conference on Composites in Infrastructure (ICCI 1996). Tucson, AZ, USA: ICCI; 1998.
- [54] Mirmiran A, Yuan W, Chen X. Design for slenderness in concrete columns internally reinforced with fiber-reinforced polymer bars. ACI Structural Journal. 2001;98.
- [55] Zadeh HJ, Nanni A. Design of RC columns using glass FRP reinforcement. Journal of Composites for Construction. 2013;17:294-304.
- [56] Afifi MZ. Behavior of circular concrete columns reinforced with FRP bars and stirrups [PhD Thesis]. Quebec, Canada: University of Sherbrooke; 2013.
- [57] Saatcioglu M, Razvi SR. Strength and ductility of confined concrete. Journal of Structural Engineering. 1992;118:1590-607.
- [58] Sharma UK, Bhargava P, Kaushik S. Behavior of confined high strength concrete columns under axial compression. Journal of Advanced Concrete Technology. 2005;3:267-81.
- [59] Paultre P, Légeron F. Confinement reinforcement design for reinforced concrete columns. Journal of structural engineering. 2008;134:738-49.
- [60] Yong Y-K, Nour MG, Nawy EG. Behavior of laterally confined high-strength concrete under axial loads. Journal of Structural Engineering. 1988;114:332-51.
- [61] Kent DC, Park R. Flexural members with confined concrete. Journal of the Structural Division. 1971;97:1969-90.
- [62] ACI 318-11. Building code requirements for structural concrete and commentary. Farmington Hills, MI, USA: American Concrete Institute; 2011.

[63] Popovics S. A numerical approach to the complete stress-strain curve of concrete. *Cement and concrete research*. 1973;3:583-99.

[64] Han B-S, Shin S-W, Bahn B-Y. A model of confined concrete in high-strength reinforced concrete tied columns. *Magazine of concrete research*. 2003;55:203-14.

[65] Tavassoli A. Behaviour of GFRP-reinforced concrete columns under combined axial load and flexure [Master's Thesis]. Toronto, Canada: University of Toronto; 2013.